HHS Public Access

Author manuscript

Acta Biomater. Author manuscript; available in PMC 2020 February 01.

Published in final edited form as:

Acta Biomater. 2019 February ; 85: 282–293. doi:10.1016/j.actbio.2018.12.051.

Mineralized nanofiber segments coupled with calcium-binding BMP-2 peptides for alveolar bone regeneration

Sunil Kumar Boda[a], **Yosif Almoshari**[b], **Hongjun Wang**[a], **Xiaoyan Wang**[b], **Richard A. Reinhardt**[c], **Bin Duan**[d], **Dong Wang**[b], **Jingwei Xie**[a,*]

[a]Department of Surgery-Transplant and Mary & Dick Holland Regenerative Medicine Program, College of Medicine, University of Nebraska Medical Center, Omaha, Nebraska 68198, United States

[b]Department of Pharmaceutical Sciences, College of Pharmacy, University of Nebraska Medical Center, Omaha, Nebraska 68198, United States

[c]Department of Surgical Specialties, College of Dentistry, University of Nebraska Medical Center, Omaha, Nebraska 68198, United States

[d]Division of Cardiology, Department of Internal Medicine and Mary & Dick Holland Regenerative Medicine Program, College of Medicine, University of Nebraska Medical Center, Omaha, NE 68198 United States

Abstract

Bone loss around tooth extraction sites can occur, thus making future placement of dental implants difficult. Alveolar bone regeneration can be guided by the application of a nanofibrous bone graft coupled with osteoinductive proteins/peptides, following tooth loss or tooth extraction. In the present study, we demonstrate the potential of mineralized nanofiber segments coupled with calcium-binding bone morphogenetic protein 2 (BMP-2) mimicking peptides for periodontal bone regeneration. Thin electro-spun nanofiber membranes of PLGA-collagen-gelatin (2:1:1 wt ratios) were mineralized in 10× modified simulated body fluid (10× mSBF) and cryocut to segments of 20 μm. For predetermined weights of the mineralized nanofiber segments, it was possible to load various amounts of heptaglutamate E7-domain-conjugated BMP-2 peptide. Mineralized short fiber grafts (2 mg), with and without E7-BMP-2 peptides, were implanted into 2 mm × 2 mm (diameter × depth) critical-sized socket defects created in rat maxillae, following extraction of the first molar teeth. A sustained release profile of E7-BMP-2 from the mineralized nanofiber segments was recorded over 4 weeks. X-ray microcomputed tomography (μ-CT) analysis of peptide-loaded nanofiber graft filled defects revealed ~3 times greater new bone volume and bone mineral density over 4 weeks in comparison to unfilled control defects. Further, histopathology data confirmed the formation of greater new osseous tissue in the BMP2 peptide-loaded, mineralized nanofiber segment group than that of fibrous connective tissue in the unfilled defect group. Altogether, the

*Corresponding author. jingwei.xie@unmc.edu (J. Xie).

Disclosures

There are no conflicts of interest relating to this work.

Appendix A. Supplementary data

Supplementary data to this article can be found online at https://doi.org/10.1016/j.actbio.2018.12.051.

mineralized nanofiber segments coupled with E7-BMP-2 peptides may be an effective treatment option for alveolar bone loss and defects.

Keywords

Alveolar bone regeneration; Mineralization; Electrospinning; Nanofiber segments; E7-BMP-2 peptides

1. Introduction

The issue of bone loss in the oral cavity continues to be a perennial problem, especially in the older populations [1]. One of the primary causes for bone loss in the oral cavity is periodontitis. A recent survey report on the prevalence of periodontitis gave an estimate of 1 in 2 adults aged ≥30 years suffering chronically from the disease [2]. Bacterial infection and host response inflammation during periodontitis can lead to erosion of the alveolar bone that supports the teeth, periodontal ligaments, and adjacent soft tissue [3], thus leading the tooth to become nonfunctional. The removal of the infected tooth can further lead to resorption of the alveolar bone [4]. As bone is a mechanosensitive tissue, the lack of masticatory function at the site of tooth loss can lead to bone resorption resulting from disuse atrophy [5]. Diabetes mellitus is another factor that increases the risk of alveolar bone resorption due to the activation of osteoclasts in the periodontium [6]. In the light of the limited availability and donor site morbidity of autografts, as well as poor bone healing potential of allografts, it is important to develop synthetic biomaterial grafts for the regeneration of maxillary and mandible bone tissues. Further, the flat bones of the jaws and skull directly form the bone tissue by the differentiation of mesenchymal stem cells into osteoblasts [7], with healing rates twice as slow as the long tibial bone for identical defect sizes [8]. Therefore, it is imperative that synthetic bone graft materials must be designed with suitable degradation rates and osteoinductive properties to accelerate the regeneration of the alveolar bone tissue.

Tissue engineering holds great promise for the healing of alveolar bone defects. The current biomaterial-based strategies for alveolar regeneration include a combination of growth factor delivery, such as enamel matrix derivative (EMD), platelet-derived growth factor (PDGF), bone morphogenetic protein-2 (BMP-2), and fibroblast growth factor-2 (FGF-2), apart from cell therapy by somatic/adult stem cells [9]. On the basis of the understanding that tissue regeneration occurs in two phases – proliferation and differentiation – a dual sequential delivery of PDGF and simvastatin from core-shell microspheres was employed for the regeneration of the periodontal bone tissue, *in vivo* [10]. In another work, the anti-inflammatory drug ibuprofen encapsulated in the electrospun poly(ε-caprolactone) (PCL) nanofiber membrane was applied to prevent periodontal inflammation-triggered bone resorption [11]. As noted earlier, diabetes mellitus is another health condition that generates a pro-inflammatory environment in the periodontal defect sites, thus leading to bone loss. To address such complications in diabetic patients, interleukin 4 (IL4) was incorporated in heparin-modified gelatin nanofibrous microspheres for switching the pro-inflammatory M1 macrophage into pro-healing/anti-inflammatory M2 macrophage phenotype [12]. Such an

osteoim-munomodulatory biomaterial system reduced inflammation and enhanced dentoalveolar bone formation in diabetic rats.

With regard to bone tissue engineering of the maxilla/mandible devoid of autologous stem cells, a combination of bioresorbable polymer and bioactive calcium phosphates (CaPs) loaded with osteoinductive factors are interesting options. A biphasic gelatin-hydroxyapatite-β-tricalcium phosphate (gelatin-HA/β-TCP) porous cryogel composite infused with BMP-2 protein-loaded poly(D,L-lactide-*co*-glycolide) (PLGA) microspheres facilitated alveolar ridge augmentation *in vivo* [13]. In another work, biphasic scaffolds of PCL-HA 3D constructs fabricated by rapid prototyping reinforced in a chitosan-poly-glycolic acid hydrogel exhibited adequate swelling and osteogenic and antibacterial properties as necessary for alveolar regeneration [14]. With particular reference to electrospun nanofibers, few studies have demonstrated their use as barrier membranes for guided tissue regeneration (GTR), wherein the barrier membrane separates the epithelium of the gingiva from the connective tissue for promoting the regeneration of the periodontal tissue. Random and aligned electrospun chitosan nanofiber membranes supported matrix deposition by human embryonic stem cell-derived mesenchymal progenitor cells, thus indicating their potential application for GTR by acting as a barrier to the gingival epithelium migration into the periodontal defect site [15]. Fused deposition modeling (FDM)-derived PCL-β-TCP scaffold and PCL electrospun membrane were press-fit into composite biphasic scaffolds and cultured with osteoblasts and periodontal ligament (PDL) cell sheets. The cell-loaded scaffolds were transferred into dentin slices and further subcutaneous implantation led to the deposition of the thin cementum-like tissue on the dentin as necessary for the regeneration of the periodontal tissue [16]. As against the complex methods adopted in the afore-mentioned studies, the present study investigates the potential of mineralized electrospun nanofiber fragments coupled with calcium-binding osteoinductive peptides for the regeneration of oral alveolus. While the inflammatory response, ectopic bone formation, and cancer risks of the whole-BMP-2 protein may pose complications in bone healing [17], we investigate the efficacy of E7-conjugated BMP-2-mimicking peptides for alveolar bone defect repair.

2. Materials and methods

2.1. Materials

PLGA with lactide-to-glycolide monomer ratio of 50:50 was procured from LACTEL (absorbable polymers, Mw 30,000–60,000); Type I collagen (calf-skin lyophilized) from Elastin Products Co., Inc, Owensville, USA; Gelatin Type A (from porcine skin powder) from Sigma-Aldrich; Hexafluoroisopropanol (HFIP) from Acros; and glutaraldehyde (GA) 25 wt% in ethanol. E7-BMP-2 Peptide (EEEEEEEKIPKASSVPTELSAISTLYL, 3022.28 g mol^{-1}) and E7-BMP-2-fluorescein isothiocyanate (FITC) (EEEEEEEKIPKASSVPTELSAISTLYL-FITC, 3524.82 g mol^{-1}) were custom synthesized and characterized by GenScript Co., Inc.

2.2. Fabrication of thin PLGA/collagen/gelatin (PCG) electrospun nanofiber membranes

The fabrication of PCG electrospun nanofiber membranes is similar to that reported in our previous publication [18]. The electrospinning solution was prepared by mixing 0.750 g of PLGA (50:50), 0.375 g of type I collagen, and 0.375 g of gelatin Type A in 20 mL of HFIP overnight. The solution was subsequently stored at 4 °C. For fabricating thin PCG nanofiber membranes, electrospinning was performed for 1 h with typical electrospinning parameters of 15 kV applied DC voltage, flow rate of 0.4 mL/h, and distance of 20 cm between the spinneret and the rotating mandrel. The nanofiber membrane was carefully removed from the collecting mandrel and cross-linked using GA vapors from a 25 wt% ethanolic solution for 24 h.

2.3. Biomineralization of PCG nanofiber membranes in simulated body fluid (SBF)

To increase the surface density of polar functional groups, the cross-linked PCG nanofiber membranes were treated with air plasma under vacuum for 1 min each on either side. Subsequently, the nanofiber membranes were immersed in a modified 10× SBF solution, the composition of which is described in one of our previous publication [19]. A supersaturated solution of the 10× SBF solution was prepared by dissolving NaCl (1000 mM), $CaCl_2$ (25 mM), and $NaH_2PO_4{\cdot}2H_2O$ (10 mM) in deionized water. Approximately 30 mg of the PCG nanofiber membrane was immersed in 100 mL of 10× SBF containing 42 mM of $NaHCO_3$. The mineralization of the PCG nanofiber membrane was performed at 37 °C, with slow stirring of the SBF solution for ~16 h. The mineralized membranes were rinsed thoroughly in D.I. water several times to detach any precipitates and freeze-dried before SEM characterization.

2.4. Preparation of short nanofiber fragments and their loading and release studies with the E7-BMP-2-FITC peptide

The mineralized PCG nanofiber membranes were frozen in water at −80 °C and cryocut at −20 °C to segments of 20 μm thickness. The cryocut mineralized PCG segments were freeze-dried to obtain the short nanofiber fragments for peptide loading and further *in vivo* studies. Both the E7-BMP-2 peptides (without and with FITC labeling) were reconstituted at 1.0 mg/mL in Tris-buffered saline (TBS; pH = 7.4). For the quantification of peptide loading and release kinetics, predetermined weights of mineralized PCG nanofiber fragments were incubated in 100 μg/mL of the E7-BMP-2-FITC peptide (Peptide:FITC = 1:1) in TBS for 24 h at room temperature. The difference in the peptide concentration before and after incubation of the mineralized PCG fragments was determined to estimate the peptide loading. The peptide release from the mineralized nanofiber fragments was recorded by measuring the fluorescence intensities of the buffer aliquots at regular intervals using excitation and emission filters of 485 and 528 nm, respectively.

2.5. Characterization of the mineralized PCG nanofiber membranes and cryocut fragments

The surface morphology of the electrospun PCG nanofiber membrane, mineralized PCG membrane, and mineralized cryocut fragments was characterized by scanning electron microscopy (FEI Quanta 200). The samples were mounted on double-side conductive carbon

tape and sputter coated with a Au-Pd target at 15 μA for 5 min. The SEM images were acquired at accelerating volt-ages of 20–25 kV. For analysis of the mineral composition on the nanofiber fragments, elemental analysis was performed using energy dispersive X-ray spectroscopy (EDAX). Additionally, the phase composition of the mineral coating on the PCG nanofiber fragments was characterized by X-ray diffraction (XRD). The mineralized PCG fragments were either crushed into fine powders without any heat treatment or calcined at 300 °C/500 °C for 5 h, at a heating rate of 2 °C/min. The fine powder samples were used for the XRD experiments, which were performed using a Rigaku Smart Lab diffractometer in Bragg-Brentano geometry, Cu Kα X-ray source (1.5418 Å), with 40 KV, and 44 mA setting. The data were collected in the interval of 0.02-degree steps, in the 2θ range of 10–90° at the scan rate of 3°/min. A D/tex Ultra 250 Silicon strip detector was used in 1D-scannig mode to collect the scattered X-ray intensity. Further, the E7-BMP-2-FITC peptide-loaded mineralized PCG nanofiber fragments were characterized by fluorescence microscopy (Zeiss).

2.6. Cytotoxicity assessment of cryocut nanofiber fragments

The potential cytotoxicity of the cryocut nanofiber fragments was assessed by the MTT assay. L929 mouse aerolar fibroblasts were procured from the American Type Culture Collection (ATCC) and revived in Eagle's minimum essential medium supplemented with 10% horse serum. The cells were expanded and maintained in the above complete media in a CO_2 incubator at 37 °C, 95% relative humidity, and 5% CO_2. For the cytotoxicity assessment, the following experimental groups were evaluated: (i) PCG NF fragments, (ii) E7-BMP-2 peptide (100 μg/mL)-loaded PCG NF fragments, (iii) Mineralized PCG NF fragments, and (iv) E7-BMP-2 peptide (100 μg/mL)-loaded mineralized PCG NF fragments.

The cytotoxicity assessment was carried out in accordance with the guidelines set by ISO 10993–5: 'Tests for Cytotoxicity – *In Vitro* Methods' in the direct contact exposure method. For the experiments, 1, 2, and 5 mg of the NF fragments from each of the 4 groups were co-cultured with L-929 mouse fibroblasts in a 0.1 wt % agar-coated 24-well plate at a seeding density of 2.5×10^4 cells/well. After 3 days of culture, complete media containing 15% (v/v) of (3-(4,5-dimethylthiazol-2-yl)-2,5-diphenyltetrazolium bromide media or MTT (5 mg/mL) was replenished and incubated for 4 h. Subsequently, the medium was removed and the formazan crystals were solubilized in 200 μL of dimethyl sulfoxide (DMSO). The absorbance of the purple formazan was measured at 490 nm using a multimode microplate reader (BioTek Synergy H1 Hybrid).

2.7. Alveolar bone defect study

As our previous study elucidated the potency of the E7-BMP-2 peptide released from 3D hybrid nanofiber aerogels in inducing cranial bone formation in rat calvarial defects [18], in the present study, we have therefore subsequently tested the efficacy of similar calcium-binding BMP-2 peptide-loaded mineralized PCG nanofiber fragments for alveolar bone regeneration *in vivo.*

2.7.1. Critical-sized alveolar defect model—All the animal experiments performed in this study followed the animal experimentation protocols approved by the Institute

Animal Care and Use Committee (IACUC) of the University of Nebraska Medical Center. A standardized tooth extraction rodent model was used, and postextraction graft procedures as detailed in the recent publication were followed in the present study [20]. Ten- to twelve-month-old female retired-breeder female Sprague Dawley rats were used as the animal model for the periodontal defect study. Before the surgery, the rats were acclimatized to the animal housing facility cages and fed on standard laboratory diet at ambient humidity and temperature. The surgery was performed in rats under general anesthesia using the nose cone method to deliver ~2% isofluorane/100% O_2. Before the extraction of the first molar tooth (M1) from the rat maxillae, local anesthesia of 0.1 mL of 3% carbocaine in 1:20,000 neocobefrin was injected into the maxillary vestibule adjacent to the M1. Following the removal of the M1 tooth on both sides, the socket was enlarged to a critical-sized defect of 2 mm diameter 2 mm depth in the maxillary bone with the help of a dental bur of 2 mm diameter under saline irrigation. The defects were either filled with graft materials for the experimental groups or left unfilled for the control group. The defects were subsequently closed by carefully suturing the adjacent soft tissue using a #6/0 line, followed by the application of a cyanoacrylate bioadhesive/bioglue (PeriAcryl 90, GluStitch, Delta, BC) to hold the graft in place. Post-surgery, 0.01 mg/kg dose of buprenorphine opioid was administered subcutaneously. Fig. 4A–C shows intraoperative images of the periodontal defect creation in the rat maxillae (upper jawbone), filling of the defect with mineralized nanofiber graft, and surgical suturing of the tissue adjacent to the defect to hold the graft in place. A total of 9 rats divided into 3 groups with two defects per rat were used for the animal experiments. The three experimental groups are as follows – (i) Unfilled defect/ control, (ii) 2 mg of mineralized PCG nanofiber fragments, and (iii) 2 mg of E7-BMP-2 peptide-loaded mineralized PCG nanofiber fragments. For a critical-sized defect of 2 mm 2 mm (diameter × depth), it was possible to fill only up to 2 of mineralized PCG NF fragments as determined in our pilot study. Therefore, 2 mg of the fiber fragments was used for the subsequent *in vivo* experiments. Postsurgery, after allowing 4 weeks for defect healing, the rats were euthanized by CO_2 asphyxiation and the rat maxillae were retrieved and fixed in 10% formalin for 3 days. The tissues were then transferred to 70% ethanol for radiographic and histological examination.

2.7.2. Radiographic analysis—The formalin-fixed maxillae were scanned with a high-resolution X-ray micro-CT scanner (SkyScan 1172, Kontich, Belgium) using a tube voltage of 70 kV, current of 141 μA, and a slice thickness/slice increment of 8.71 μm. The analysis of the micro-CT data was performed using CT analyzer software (Brucker microCT). From the multiple scan slices, a 3D reconstruction was performed for each of the two sides of the rat maxillae. For evaluating new bone formation in the maxilla, the coronal image slices were 3D reconstructed. The region of interest (ROI: 2 mm diameter × 2 mm depth) was selected in the area anterior to the roots of the second molar tooth (M2), where the critical-sized 2 mm defect was made for the surgery. The coronal view micro-CT image of the maxilla immediately after defect creation also aided in locating the defect site. In the ROI delineated by dashed circles, 3D reconstruction of the coronal images was performed using CT SkyScan software. For the 3D reconstruction, ~200 coronal (XZ) slices from the cementum–enamel junction (CEJ) below into the alveolar bone were used. From the circular

defect regions, the new bone volume percentage, bone mineral density, and trabecular bone parameters (trabecular thickness, number, and separation) were determined.

2.7.3. Histopathological analysis—Subsequent to acquiring the data for radiographic analysis, the rat maxillae were immersed in decalcification buffer, i.e., Rapid Cal Immuno (BBC Biochemical, Mount Vernon, WA) for 2 weeks. The decalcification buffer was aspirated and replenished every 2 days for the 2-week period. Following decalcification, the maxilla was bisected as two halves, dehydrated with an increasing gradient of ethanol series (70–100%), and embedded in separate paraffin wax blocks. From the embedded tissue blocks, tissue sections of 4 μm thickness were prepared using a microtome. Several sections were prepared for each sample and stained with hematoxylin and eosin (H&E) or Masson's trichrome, following the instructions provided by the manufacturer. The stained sections were examined using a Ventana's Coreo Au slide scanner 3.1.3. Using Ventana image viewer v. 3.1.3, representative snapshots were taken at 2× and 10× magnification.

2.8. Statistical analysis

IBM SPSS Statistics software 20 was employed for statistical analysis of data presented in the current study. All data are presented as mean ± standard deviation of n = 6 replicates per group. One-way analysis of variance (ANOVA) with the Tukey test was performed to assess statistical significance at $p < 0.05$, where p denotes the probability that there is no significant difference between the mean values of the compared groups.

3. Results

3.1. Morphology of mineralized PCG membrane and cryocut nanofiber fragments

As mentioned in the introduction, growth factor and anti-inflammatory cytokine-loaded microspheres have been previously studied for the regeneration of the periodontal/alveolar bone tissue. On similar lines, the current study is the first report on the application of mineralized short nanofiber fragments coupled with osteoinductive peptides for periodontal bone tissue engineering. Fig. 1 is a schematic illustration showing the application of mineralized nanofiber segments loaded with the E7-BMP-2 peptide for the healing of critical-sized (2 mm diameter × 2 mm depth) defects in rat maxillae. The morphology of the electrospun PCG nanofiber membrane before and after mineralization in modified 10× SBF was studied by SEM. Using Image J, the diameters of the GA cross-linked electrospun PCG nanofibers were in the range of 249 ± 112 nm (Fig. 2A). Further, it is well known that as the thick-ness of the nanofiber membrane increases with the duration of electrospinning, the porosity of the membrane is drastically reduced. It was shown that the pore size reduced significantly from ~35 μm to 0.9 μm in PCL-collagen nanofiber membrane for electro-spinning duration from 10 to 40 s under typical operating parameters of 10–15 kV DC voltage, flow rate of 0.6 mL/h, and spinneret-to-collector distance of 10 cm [21]. Such a decrease in porosity was shown to hinder cellular infiltration into the membrane. In our study, the biomineralization of electrospun nanofibers was observed predominantly on the surface of thick nanofiber membranes due to the low membrane porosity. There-fore, thin nanofiber membranes were electrospun for 1 h to ensure maximal coverage of the membrane with CaP minerals. The diameters of the PCG nanofibers increased from 249 ± 112 nm to

1758 ± 346 nm upon mineralization overnight in 10× SBF for 16 h. A flaky apatite-like mineral coating morphology was seen on the mineralized fiber membrane (Fig. 2B), which was retained after cryocutting to 20 μm thick fragments (Fig. 2C and 2D). Because of the large amount of mineral deposition on the membrane, the fiber fragments are aggregates of nanofibers within the 20 μm segments and not dispersed as individual mineralized fibers.

3.2. Elemental and phase composition of the mineral coating on PCG nanofiber fragments

The composition of the mineral coating on the PCG nanofiber fragments was characterized by EDAX. Fig. S1 shows the elemental mapping of the mineralized nanofiber fragments. As expected, X-ray signals were detected for calcium (Ca), phosphorus (P), and oxygen (O) from the flaky mineral coating. Fig. S2 corresponds to a line scan across the mineralized nanofiber fragments, which semiquantitatively provides information about the order of elemental abundance (wt%) in the mineral coating, i.e., Ca > P > O. A quantitative assessment of the mineral coating was obtained by point scan at different locations on the mineral coating. Fig. 2E shows the point probe (shown in the inset) EDAX spectrum of the mineralized nanofiber fragments. The EDAX spectrum shows all the signals identified in the elemental mapping and line scan along with additional signal from the Al foil on which the sample was mounted. From the peak areas in the EDAX spectra, the molar ratio of Ca/P was ascertained to be 1.65 ± 0.06, which is close to a Ca/P ratio of 1.67 in hydroxyapatite (HA). Further, the XRD data of the mineralized PCG nanofiber fragments without and with heat treatment discerned characteristic peaks for hydroxyapatite (Fig. S3). The mineralized fiber fragments without heat treatment exhibited a broad amorphous hump at lower angles (2θ = 10–25°) because of the polymer backbone. At 300 °C and 500 °C, calcination removed the amorphous polymer content leading to more intense crystalline peaks of hydroxyapatite. Further, no phase transformation of the hydroxyapatite mineral coating was detected due to the low calcination temperatures [22]. Thus, the mineral coating on the PCG nanofiber fragments was ascertained to be flaky HA.

3.3. Loading and release of the E7-BMP-2-FITC peptide from mineralized PCG nanofiber fragments

As performed in our previous study, the loading and release of the E7-BMP-2 peptide from the mineralized nanofiber fragments was quantified by measuring the fluorescence intensity of the FITC peptide analog in Tris-buffer saline [18]. At a peptide concentration of 100 mg/mL, the loading of the mineralized nanofiber fragments increased proportionately to the weight of the mineralized PCG fragments. For 1, 2, and 5 mg of mineralized PCG nanofiber fragments, Ì33, Ì50, and Ì90 mg of the peptide loading was recorded, respectively (Fig. 3A). Sustained release profiles of the peptide were recorded for all the three peptide loadings (Fig. 3B), with >95% of the peptide released within 4 weeks. Fig. 3C and D are representative fluorescence micrographs of the E7-BMP-2-FITC peptide-loaded nanofiber fragments, immediately after loading and after 4 weeks of release, respectively. The slow dissolution of CaP minerals from the mineralized nanofiber fragments in the Tris-buffer supposedly facilitates the sustained release of the pep- tide. Additionally, the loading and release profiles of the E7-BMP-2 peptide for 5 mg of each of the mineralized and nonmineralized PCG NF fragments were compared. Fig. S4A indicates that a much higher

amount of the E7-BMP-2 peptide (3 times) can be loaded onto the mineralized PCG fragments than onto the PCG fragments. Additionally, the peptide release for the PCG fragments exhibited a burst release profile, with >95% of the peptide released within 24 h, whereas a similar percentage was released within 1 week in case of the mineralized PCG fragments. Thus, a controlled release of the E7-BMP-2 peptide from the mineralized PCG NF fragments can be ascertained.

3.4. Cytocompatibility of cryocut nanofiber fragments in vitro

A dose-dependent cytotoxicity evaluation of the cryocut nano- fiber fragments with L929 mouse fibroblasts revealed favorable cytocompatibility of all the 4 experimental groups with regard to the control tissue culture polystyrene (TCPS) after 3 days of culture. A close observation of the results in Fig. S5 indicates a composition and dose-dependent variation in cell viability. Except for the PCG NF fragments, all the other experimental groups elicited a dose-dependent variation in cell viability (although not statistically significant between the doses). Particularly, at a low dosage (1 mg), the E7-BMP-2-loaded mineralized PCG NF fragments elicited lower cellular activity (although not statistically significant with regard to TCPS control), which was revived at 2 mg and significantly higher than that of control at 5 mg. In fact, the viability and proliferation of the fibroblasts co-cultured with the PCG NF fragments and the E7-BMP-2 peptide-loaded mineralized NF fragments were significantly higher than the TCPS control. As the doubling time of L929 fibroblasts was 21–24 h and the MTT assessment was performed after 3 days of co-culture, the results also reflected on the proliferation effects of the PCG NF fragments. Further, several literature reports elucidate enhanced cell proliferation on nanofiber matrices over conventional 2D flat substrates/films using the MTT assay [23], and our results resonate with those studies. In Fig. S5, the cellular activity seems to increase with an increase in the dosage of the NF fragments. This indicates a potential mitogenic effect of the cryocut NF fragments on the aerolar mouse fibroblasts. Such a cell proliferative effect can aid in wound healing and defect closure in vivo. In contrast to cellulose nanofibrils that induced apoptosis and activated cellular stress genes in bovine fibroblasts at doses >0.2 mg/mL [24], the cryocut short NF segments in the present study are cytocompatible even at exposure doses of 2 and 5 mg/mL.

3.5. Alveolar bone regeneration in vivo

Our previous study demonstrated the efficacy of a BMP-2- mimicking peptide-loaded PCG-containing nanofiber aerogel for cranial bone regeneration in 8 mm rat calvarial defects [18]. There- fore, in the current study, a similar PCG nanofiber composition was chosen for apatite mineralization, and the mineralized nanofiber fragments were coupled with the calcium-binding E7-BMP-2 peptide for the alveolar bone regeneration in 2 mm critical-sized defects. Following tooth extraction, drilling of critical-sized defects, surgical placement of the mineralized graft, and defect closure by suturing, a small dip in the body weight of the rats was recorded for the first week postsurgery (data not shown). This can be ascertained by the inability of the rats to consume even softened “ad libitum” due to the initial inflammation that incurred during the surgery. The initial inflammatory response arose because of the tooth extraction followed by further drilling of the maxillary bone underneath to create critical-sized defects. This initial inflammation lasted for 2–3 days postsurgery and therefore did not correspond to the side effects generated by BMP-2-mimicking peptides.

Nevertheless, the rat body weights resumed to a normal increase from the second week up to 4 weeks.

3.5.1. Micro-CT analysis—Micro-CT was employed to quantify the extent of bone regeneration after 4 weeks of mineralized PCG graft implantation in rat maxillae, following extraction of the first molar tooth (M1). Representative 3D reconstructions of the coronal (XZ)-view micro-CT images for the different implant groups are shown in Fig. 4D–G, with the regions of interest being demarcated in dashed circles. It may be noted that Fig. 4D and E correspond to micro-CT images of the control unfilled defect group, immediately after defect creation and 4 weeks after surgery, respectively. Fig. 4H is a statistical analysis of the new bone volume percentage (BV/TV in %) and bone mineral density (BMD in g/cc) measured in the different experimental groups. The E7-BMP-2 peptide-loaded mineralized nanofiber graft alone exhibited significantly greater X-ray radiopacity within the ROI than the unfilled defect. This suggests larger new bone volume fraction (%) and bone mineral density (g/cc) of the E7-BMP-2 peptide-coupled mineralized PCG nanofiber fragments. Further, the trabecular parameters of the spongy alveolar bone tissue formed in the maxillary circular defects were determined (Fig. 4I). While the trabecular thickness (Tb.Th in mm) and the trabecular separation (Tb.Sp in mm) were similar between the experimental groups, the trabecular number (Tb.N in 1/mm) for the E7-BMP-2 peptide-loaded mineralized PCG group was significantly larger than that of the control/unfilled defect group. Although the mineralized PCG grafts without the BMP-2 peptide seemed to elicit better new bone formation than the control, no statistical significant difference was noted at $p < 0.05$. Overall, the osteoinductive efficacy of the mineralized short nanofiber grafts coupled with calcium binding BMP-2-mimicking peptides for alveolar bone healing can be ascertained. It is also possible that the nonresorbed mineral coating on the nanofiber fragments can contribute to the contrast in the X-ray micro-CT. To ascertain this, histological analysis of the tissue sections from the three experimental groups was undertaken. To facilitate easy comparison with the sagittal plane histological sections, representative sagittal (YZ) view micro-CT images are shown in Fig. S6.

3.5.2. Histopathological analysis—Postdecalcification of the retrieved rat maxillae, tissue sections of the different experimental groups were analyzed by H&E and Masson's trichrome staining. Fig. 5A1–D2 and Fig. 6A1–D2 are representative H&E and Masson's trichrome-stained images for the various experimental groups, respectively. In both the figures, Figs. 5A1/A2 and 6A1/A2 correspond to the tissue section immediately after first molar extraction (M1) and defect creation in the maxillary bone. These images have been shown to demarcate the defect location adjacent to the second molar tooth (M2). The initial inflammation of the oral cavity observed after surgery completely subsided after 4 weeks of graft implantation. Importantly, no apparent inflammatory or foreign body reaction was observed in any of the experimental groups at 4 weeks. Both H&E and trichrome staining suggested retarded new bone formation and greater fibrous connective tissue in the unfilled defect/control group (Figs. 5B1/B2 and 6B1/B2). On the other hand, the mineralized fragmented nanofiber graft group revealed sparsely formed new bone. The new bone formation was localized to the periphery of the defect region in case of the mineralized nanofiber fragments devoid of the E7-BMP-2 peptide (Figs. 5C1/C2 and 6C1/C2). In the

peptide-loaded mineralized fragmented nanofiber group, greater new bone tissue was observed in the center of the defect (Figs. 5D1/D2 and 6D1/D2). However, the maxillary bone defects filled with the mineralized grafts did not elicit significant soft/fibrous connective tissue infiltration unlike the control unfilled defect. The nanofiber fragments may have inhibited soft fibrous and/or epithelial tissue invasion into the defect region while enhancing the osteoblastic cell migration into the defect region. This is consistent with an earlier report of enhanced migration and clustering of osteoblast-like cells on inorganic bone mineral (ABM) particles coated with a P-15 collagen-mimicking peptide suspended within hyaluronic acid hydrogels [25]. Therefore, the biomimetic mineralized nanofiber fragments create an osseous tissue-like microenvironment for greater infiltration of boneforming cells into the defect location. Overall, the histology and micro-CT analysis together indicate the maximum osteoinductive potency of the E7-BMP-2 peptide-loaded mineralized nanofiber fragments for alveolar bone regeneration.

4. Discussions

There is tremendous potential for tissue engineering applications of short electrospun nanofiber fragments, which are largely uninvestigated. The injectability of the short nanofiber fragments present several advantages compared to their precursor 2D electrospun nanofiber membranes/mats. The different methods and ease of the fabrication of nanofiber fragments by electric spark generation during electrospinning, cryogenic cutting, and probe ultrasonication have been deliberated in a recent review [26]. Depending on the brittleness/ductility of the polymer, one of the aforementioned methods may be employed for the generation of short electrospun nanofiber fragments. Using a unique method, short nanofiber fragments of poly (glycerol sebacate) (PGS) were fabricated from coaxial electrospun fibers of PGS core and poly-L- lactic acid (PLLA) shell by dissolving the latter in a DCM:hexane (2:1) solvent system [27]. The PGS short fibers supported the maturation of cardiomyocytes by enhancing the expression of cardiac markers – actinin, troponin, myosin heavy chain, and connexin 43 and therefore presented their potential as injectable biomaterials for treating myocardial infarction. In another work, short fibers of poly (styrene-co-maleic acid) were cryocut into lengths of 20, 50, and 80 mm, and such fiber fragments regulated spheroidal culture and function of primary hepatocytes, as testified by the responsiveness of the spheroids for the clearance of model drugs [28]. By injecting cryocut short nanofiber fragments loaded with a traditional Chinese medicine (astragalocide IV), therapeutic angiogenesis was realized by microvessel formation in the hindlimb ischemic nude mice model [29]. On similar lines, the present study investigates the potential application of mineralized nanofiber fragments coupled with calcium-binding BMP-2-mimicking peptides for alveolar bone regeneration.

With particular reference to alveolar bone tissue engineering, peptide-, protein-, and/or growth factor-loaded microparticles are being used to fill maxillary bone defects [10,12]. However, in the current study, mineralized short nanofiber fragments are being utilized for oral bone tissue regeneration. Apart from the biomaterial and drug/growth factor delivery characteristics, the extent of periodontal bone regeneration is also dependent on clinical factors such as the alveolar defect location, the surgical procedure, and the animal model used. Compared to the work of Chang et al., wherein PDGF and simvastatin were

sequentially delivered [10], the new bone volume (%), bone mineral density (g/cc), and trabecular bone parameters are lower in our study. This can be ascribed to difference in the creation of the maxillary bone defects, wherein maxillary defects were created immediately after the extraction of the first molar tooth, while Chang et al. let the sockets heal for 4 weeks after the molar extraction. In another work, mandibular defects created in diabetic rats showed excellent periodontal bone healing induced by IL-4 delivery from modified gelatin microspheres [12]. However, it should be noted that the mean bone mineral density (BMD) of the mandible is twice that of the maxilla, and thus, the mandible can resist bone resorption to a greater extent [30]. Next, we discuss the biomaterial and drug delivery characteristics that affect alveolar bone regeneration. A pertinent question is whether the drug carrier morphology matters in the context of tissue regeneration and which morphology is better, particles or fibers? To answer this question, FITC-tagged bovine serum albumin (BSA-FITC)-encapsulated nanoparticles and nanofibers of PLLA and m-PEG-PLLA were fabricated, respectively, and the release profiles indicated a burst release of BSA-FITC from the nanoparticles, while a slower sustained release was recorded over 10 days with nanofibers [31]. In another work, drug release and degradation profiles of electrospun poly($_{D,L}$-lactide) nanofibers could be modulated by varying the fiber diameter, thus suggesting nanofibers as alternative drug carriers compared to nanoparticles and thin films [32]. Additionally, the extracellular matrix (ECM)-mimicking topography presented by electrospun nanofibers may help elicit a more favorable tissue regeneration response. Thus, the biomimetic mineralized nanofiber fragments may be more potent for healing alveolar defects than similar micro/nanoparticles.

In the current work, the BMP-2-mimicking peptide is chemically modified by attaching a calcium-binding heptaglutamate moiety to form the E7-BMP-2 peptide. Similarly, the vascular endothelial growth factor (VEGF)-mimicking peptide (QK) was acetylated as AcQK for conjugation to the gelatin methacrylate (GelMA) hydrogel, which elicited angiogenesis by enhancing microvascularization of endothelial cells [33]. The modified E7-BMP-2 and E7-QK can be tethered to mineralized nanofiber fragments/scaffolds by calcium coupling for better regeneration of vascularized bone. Apart from the heptaglutamate E7 domain, it may also be worthwhile to investigate and compare the efficacy of octaglutamate E8, octaaspartate D8, and bisphosphonate chemical moieties conjugated to the BMP-2-mimicking peptide. All the aforementioned peptide modifications have been reported to enhance calcium binding as testified by >90% of the conjugated peptides bound to hydroxyapatite compared to <5% for the unmodified peptides [34]. Furthermore, a previous work demonstrated the preferential binding of octaaspartate D8-conjugated osteotropic peptide to bone resorption sites in ovariectomized rats [35]. Apart from therapeutic peptides, short nanofiber fragments can also be immobilized with chemotactic growth factors for bone tissue engineering applications. A protease-resistant stromal cell-derived factor-1 (SDF-1) was efficiently delivered by self- assembling nanofibers for the recruitment of stem cells, which improved heart function following myocardial infarction [36]. In another case, platelet-derived growth factor (PDGF) released from coaxial electrospun dextran core and poly($_{L}$-lactide-co-Ɛ-caprolac tone) nanofibers elicited the proliferation of vascular smooth muscle cells *in vitro* [37], while a combination of VEGF and PDGF released from multifunctional chitosan/poly(ethylene oxide) promoted skin wound healing *in vivo* [38]. In

a similar manner, an optimal combination of growth factors released from the nanofiber fragments can accelerate the recruitment and proliferation of stem/progenitor cells at the defect site followed by stem cell differentiation to osteoblasts.

Finally, the short nanofiber fragments can be consolidated into 3D nanofiber aerogel scaffolds for filling large-sized bone defects as demonstrated in our recent work [18]. In a noteworthy work, magnetic short fibers of PLGA were oriented in a hydrogel using an external magnetic field and such anisogel-induced unidirectional growth of functional nerve cells [39], as necessary for neural tissue engineering. In another recent work from our group, we demonstrate the fabrication of injectable nanofiber microspheres from short nanofiber fragments, which could be loaded with stem cells for tissue regeneration [40]. Alternately, we also intend to investigate the efficacy of strontium and copper co-doped bioactive glass nanofiber fragments, which were demonstrated to enhance osteo- genesis and angiogenesis, and inhibit osteoclastogenesis *in vitro* [41]. In summary, this is among the first reports on the potential of mineralized nanofiber fragments coupled with calcium- binding BMP-2-mimicking peptides for alveolar bone healing.

5. Conclusion

In a parallel to growth factor-loaded microspheres, the filling of alveolar bone defects with nanofiber fragments as a potential alternative for bone tissue regeneration has been demonstrated in the present study. Further, the coupling of calcium-binding osteoinductive peptides to the mineralized nanofiber fragments enabled sustained peptide release for 4 weeks. The E7-domain-conjugated BMP-2 peptide implicated in the faster healing of critical-sized maxillary defects of 2 mm diameter 2 mm depth in rats, which can be further tailored to E8, D8, D7, and bisphosphonate modifications for optimal calcium binding and new bone formation. The mineralized nanofiber fragments with the incorporation of peptides may have a great potential to regenerate craniofacial bone defects.

Supplementary Material

Refer to Web version on PubMed Central for supplementary material.

Acknowledgments

This work was supported by grants from the National Institute of General Medical Science (NIGMS) at the NIH (2P20 GM103480), the National Institute of Dental and Craniofacial Research (NIDCR) at the NIH (1R21DE027516), NE LB606, and startup funds from the Mary and Dick Holland Program at the University of Nebraska Medical Center.

References

[1]. Jeffcoat MK, Bone loss in the oral cavity, J. Bone Miner. Res 8 (1993) S467–S473. [PubMed: 8122514]

[2]. Eke PI, Dye BA, Wei L, Slade GD, Thornton-Evans GO, Borgnakke WS, Taylor GW, Page RC, Beck JD, Genco RJ, Update on prevalence of periodontitis in adults in the United States: NHANES 2009 to 2012, J. Periodontol 86 (2015) 611–622. [PubMed: 25688694]

[3]. Haze A, Taylor AL, Haegewald S, Leiser Y, Shay B, Rosenfeld E, Gruenbaum-Cohen Y, Dafni L, Zimmermann B, Heikinheimo K, Gibson CW, Fisher LW, Young MF, Blumenfeld A,

Bernimoulin JP, Deutsch D, Regeneration of bone and periodontal ligament induced by recombinant amelogenin after periodontitis, J. Cell. Mol. Med 13 (2009) 1110–1124. [PubMed: 19228267]

[4]. Hansson S, Halldin A, Alveolar ridge resorption after tooth extraction: a consequence of a fundamental principle of bone physiology, J. Dent. Biomech 3 (2012). 1758736012456543. [PubMed: 22924065]

[5]. Cohn SA, Disuse atrophy of the periodontium in mice, Arch. Oral Biol. 10 (1965) 909–919. [PubMed: 5226995]

[6]. Wu Y-Y, Xiao E, Graves DT, Diabetes mellitus related bone metabolism and periodontal disease, Int. J. Oral Sci 7 (2015) 63–72. [PubMed: 25857702]

[7]. Mackie EJ, Tatarczuch L, Mirams M, The skeleton: a multi-functional complex organ. The growth plate chondrocyte and endochondral ossification, J. Endocrinol 211 (2011) 109–121. [PubMed: 21642379]

[8]. Lim J, Lee J, Yun H-S, Shin H-I, Park EK, Comparison of bone regeneration rate in flat and long bone defects: calvarial and tibial bone, Tissue Eng. Regener. Med 10 (2013) 336–340.

[9]. Shimauchi H, Nemoto E, Ishihata H, Shimomura M, Possible functional scaffolds for periodontal regeneration, Jpn. Dent. Sci. Rev 49 (2013) 118–130.

[10]. Chang P-C, Dovban AS, Lim LP, Chong LY, Kuo MY, Wang C-H, Dual delivery of PDGF and simvastatin to accelerate periodontal regeneration in vivo, Biomaterials 34 (2013) 9990–9997. [PubMed: 24079892]

[11]. Batool F, Morand D-N, Thomas L, Bugueno IM, Aragon J, Irusta S, Keller L, Benkirane-Jessel N, Tenenbaum H, Huck O, Synthesis of a novel electrospun polycaprolactone scaffold functionalized with Ibuprofen for periodontal regeneration: an in vitro and in vivo study, Materials 11 (2018) 580.

[12]. Hu Z, Ma C, Rong X, Zou S, Liu X, Immunomodulatory ECM-like microspheres for accelerated bone regeneration in Diabetes Mellitus, ACS Appl. Mater. Interfaces 10 (2018) 2377–2390. [PubMed: 29280610]

[13]. Chang H-C, Yang C, Feng F, Lin F-H, Wang C-H, Chang P-C, Bone morphogenetic protein-2 loaded poly(D, L-lactide-co-glycolide) microspheres enhance osteogenic potential of gelatin/hydroxyapatite/b-tricalcium phosphate cryogel composite for alveolar ridge augmentation, J. Formos. Med. Assoc 116 (2017) 973–981. [PubMed: 28256366]

[14]. Dario P, Chiara M, Lucia G, Alessandro P, Giuseppantonio M, Giovanna B, Federica C, Integrated three-dimensional fiber/hydrogel biphasic scaffolds for periodontal bone tissue engineering, Polym. Int 65 (2016) 631–640.

[15]. Qasim SB, Najeeb S, Delaine-Smith RM, Rawlinson A, Ur Rehman I, Potential of electrospun chitosan fibers as a surface layer in functionally graded GTR membrane for periodontal regeneration, Dent. Mater 33 (2017) 71–83. [PubMed: 27842886]

[16]. Vaquette C, Fan W, Xiao Y, Hamlet S, Hutmacher DW, Ivanovski S, A biphasic scaffold design combined with cell sheet technology for simultaneous regeneration of alveolar bone/periodontal ligament complex, Biomaterials 33 (2012) 5560–5573. [PubMed: 22575832]

[17]. Zara JN, Siu RK, Zhang X, Shen J, Ngo R, Lee M, Li W, Chiang M, Chung J, Kwak J, Wu BM, Ting K, Soo C, High doses of bone morphogenetic protein 2 induce structurally abnormal bone and inflammation in vivo, Tissue Eng. Part A 17 (2011) 1389–1399. [PubMed: 21247344]

[18]. Weng L, Boda SK, Wang H, Teusink MJ, Shuler FD, Xie J, Novel 3D hybrid nanofiber aerogels coupled with BMP-2 peptides for cranial bone regeneration, Adv. Healthc. Mater 7 (2018) 1701415.

[19]. Weng L, Teusink MJ, Shuler FD, Parecki V, Xie J, Highly controlled coating of strontium-doped hydroxyapatite on electrospun poly(e-caprolactone) fibers, J. Biomed. Mater. Res. B Appl. Biomater 105 (2017) 753–763. [PubMed: 26743543]

[20]. Willett ES, Liu J, Berke M, Giannini PJ, Schmid M, Jia Z, Wang X, Wang X, Samson K, Yu F, Wang D, Nawshad A, Reinhardt RA, Standardized rat model testing effects of inflammation and grafting on extraction healing, J. Periodontol 88 (2017) 799–807. [PubMed: 28440741]

[21]. Babak MS, Farshid S, Yevgeniy P, Lichen W, Hongjun W, Improved cell infiltration of electrospun nanofiber mats for layered tissue constructs, J. Biomed. Mater. Res. A 104 (2016) 1479–1488. [PubMed: 26845076]

[22]. Boda SK, Anupama AV, Basu B, Sahoo B, Structural and magnetic phase transformations of hydroxyapatite-magnetite composites under inert and ambient sintering atmospheres, J. Phys. Chem. C 119 (2015) 6539–6555.

[23]. Wu S-C, Chang W-H, Dong G-C, Chen K-Y, Chen Y-S, Yao C-H, Cell adhesion and proliferation enhancement by gelatin nanofiber scaffolds, J. Bioact. Compat. Pol 26 (2011) 565–577.

[24]. Pereira MM, Raposo NR, Brayner R, Teixeira EM, Oliveira V, Quintao CC, Camargo LS, Mattoso LH, Brandao HM, Cytotoxicity and expression of genes involved in the cellular stress response and apoptosis in mammalian fibroblast exposed to cotton cellulose nanofibers, Nanotechnology 24 (2013) 075103. [PubMed: 23358497]

[25]. Nguyen H, Qian JJ, Bhatnagar RS, Li S, Enhanced cell attachment and osteoblastic activity by P-15 peptide-coated matrix in hydrogels, Biochem. Biophys. Res. Commun 311 (2003) 179–186. [PubMed: 14575711]

[26]. Chen S, Li R, Li X, Xie J, Electrospinning: an enabling nanotechnology platform for drug delivery and regenerative medicine, Adv. Drug Deliv. Rev (2018), 10.1016/j.addr.2018.05.001.

[27]. Ravichandran R, Venugopal JR, Sundarrajan S, Mukherjee S, Sridhar R, Ramakrishna S, Minimally invasive injectable short nanofibers of poly(glycerol sebacate) for cardiac tissue engineering, Nanotechnology 23 (2012) 385102. [PubMed: 22947662]

[28]. Wei J, Lu J, Liu Y, Yan S, Li X, Spheroid culture of primary hepatocytes with short fibers as a predictable in vitro model for drug screening, J. Mater. Chem. B 4 (2016) 7155–7167.

[29]. Li H, Wan H, Xia T, Chen M, Zhang Y, Luo X, Li X, Therapeutic angiogenesis in ischemic muscles after local injection of fragmented fibers with loaded traditional Chinese medicine, Nanoscale 7 (2015) 13075–13087. [PubMed: 26176198]

[30]. Devlin H, Horner K, Ledgerton D, A comparison of maxillary and mandibular bone mineral densities, J. Prosthet. Dent 79 (1998) 323–327. [PubMed: 9553887]

[31]. Shan X, Liu C, Li F, Ouyang C, Gao Q, Zheng K, Nanoparticles vs. nanofibers: a comparison of two drug delivery systems on assessing drug release performance in vitro, Des. Monomers Polym. 18 (2015) 678–689.

[32]. Cui W, Li X, Zhu X, Yu G, Zhou S, Weng J, Investigation of drug release and matrix degradation of electrospun poly(dl-lactide) fibers with paracetanol inoculation, Biomacromolecules 7 (2006) 1623–1629. [PubMed: 16677047]

[33]. Prakash Parthiban S, Rana D, Jabbari E, Benkirane-Jessel N, Ramalingam M, Covalently immobilized VEGF-mimicking peptide with gelatin methacrylate enhances microvascularization of endothelial cells, Acta Biomater. 51 (2017) 330–340. [PubMed: 28110074]

[34]. Murphy MB, Hartgerink JD, Goepferich A, Mikos AG, Synthesis and in vitro hydroxyapatite binding of peptides conjugated to calcium-binding moieties, Biomacromolecules 8 (2007) 2237–2243. [PubMed: 17530891]

[35]. Wang D, Miller SC, Shlyakhtenko LS, Portillo AM, Liu X-M, Papangkorn K, Kopecková P, Lyubchenko Y, Higuchi WI, Kopecek J, Osteotropic peptide that differentiates functional domains of the skeleton, Bioconjuguate Chem. 18 (2007) 1375–1378.

[36]. Segers VFM, Tokunou T, Higgins LJ, MacGillivray C, Gannon J, Lee RT, Local delivery of protease-resistant stromal cell derived factor-1 for stem cell recruitment after myocardial infarction, Circulation 116 (2007) 1683–1692. [PubMed: 17875967]

[37]. Li H, Zhao C, Wang Z, Zhang H, Yuan X, Kong D, Controlled release of PDGF- bb by coaxial electrospun dextran/poly(L-lactide-co-e-caprolactone) fibers with an ultrafine core/shell structure, J. Biomater. Sci. Polym. Ed 21 (2010) 803–819. [PubMed: 20482986]

[38]. Xie Z, Paras CB, Weng H, Punnakitikashem P, Su L-C, Vu K, Tang L, Yang J, Nguyen KT, Dual growth factor releasing multi-functional nanofibers for wound healing, Acta Biomater. 9 (2013) 9351–9359. [PubMed: 23917148]

[39]. Omidinia-Anarkoli A, Boesveld S, Tuvshindorj U, Rose JC, Haraszti T, De Laporte L, An injectable hybrid hydrogel with oriented short fibers induces unidirectional growth of functional nerve cells, Small 13 (2017) 1702207.

[40]. Boda SK, Chen S, Chu K, Kim HJ, Xie J, Electrospraying electrospun nanofiber segments into injectable microspheres for potential cell delivery, ACS Appl. Mater. Interfaces 10 (2018) 25069–25079. [PubMed: 29993232]

[41]. Weng L, Boda SK, Teusink MJ, Shuler FD, Li X, Xie J, Binary doping of strontium and copper enhancing osteogenesis and angiogenesis of bioactive glass nanofibers while suppressing osteoclast activity, ACS Appl. Mater. Interfaces 9 (2017) 24484–24496. [PubMed: 28675029]

Statement of Significance

With the high incidence of dental implants/fixtures for missing teeth, the success of the surgical procedures in restorative dentistry is dictated by the quality and quantity of the supporting alveolar bone. To address the problem of alveolar bone loss and defects due to tumor, periodontitis, or even postextraction remodeling, the present study is the first report on the application of mineralized nanofiber fragments coupled with calcium-binding osteoinductive BMP-2 peptides as a synthetic graft material for oral bone regeneration. The ease of fabrication and application of cryocut mineralized nanofiber fragments as maxillofacial bone defect fillers present a promising alternative to the current dental bone graft formulations. Furthermore, the nanofiber segments may also be utilized for several biomedical applications including hemostasis, soft tissue engineering, and wound healing.

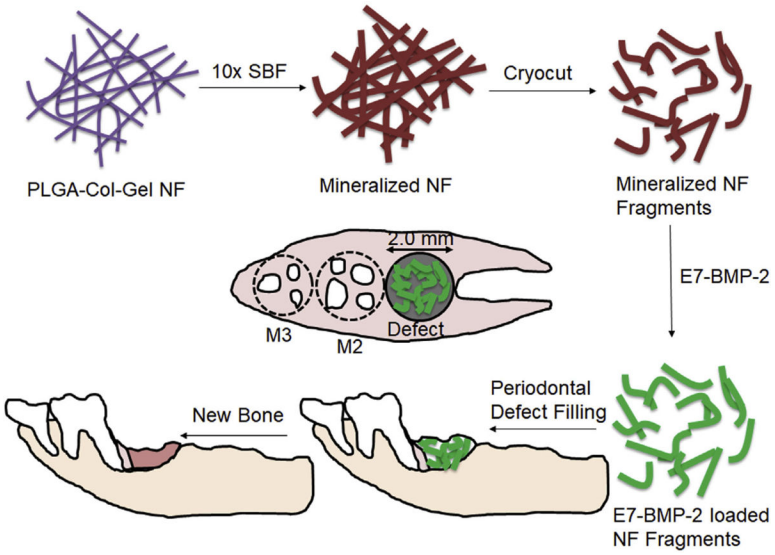

Fig. 1.

Schematic illustrating the application of mineralized nanofiber segments immobilized with calcium coupling of the E7-BMP-2 peptide for periodontal bone regeneration in maxillary defects (2 mm diameter 2 mm depth) created following the extraction of the first molar tooth (M1).

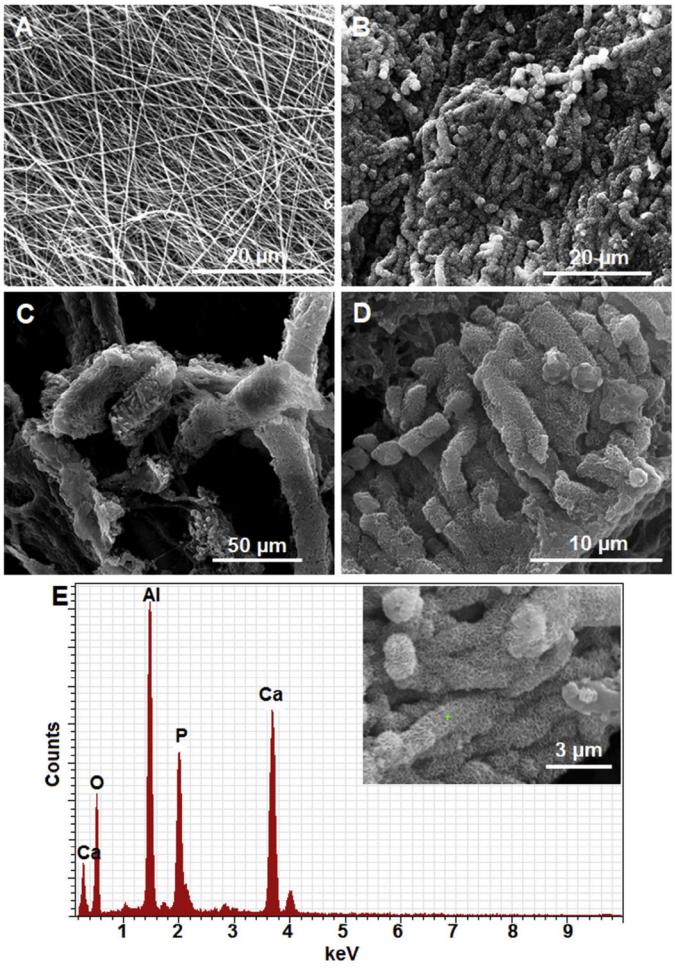

Fig. 2.

Preparation of mineralized nanofiber fragments by (A) Electrospinning of thin nanofiber membrane, (B) SBF mineralization of the membrane, and (C) Cryocutting of the mineralized nanofiber membranes to 20 mm segments. (D) Magnified image of the mineralized short nanofiber segments and (E) EDAX spectrum of mineralized nanofiber fragments.

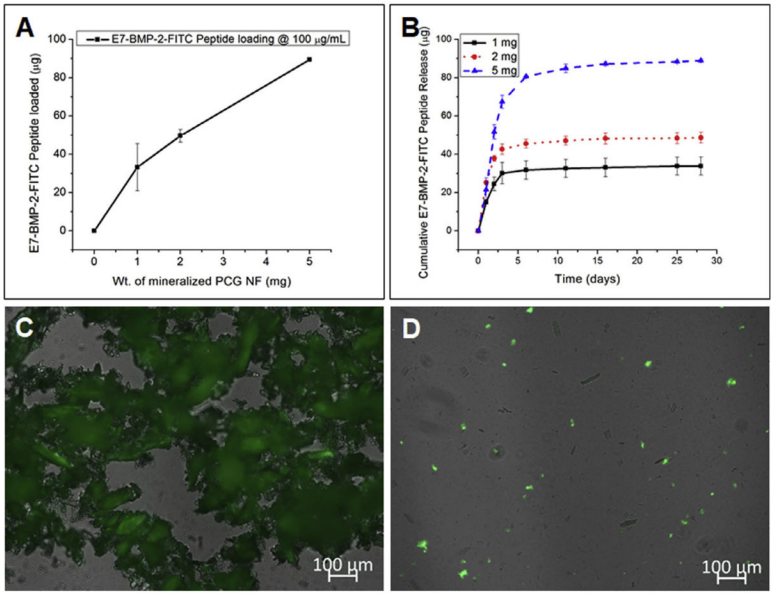

Fig. 3.

(A) Loading of the E7-BMP-2-FITC peptide on mineralized PCG NF fragments by immersing in 100 mg/mL of the peptide solution in TBS for 24 h at room temperature and (B) Cumulative release profiles over 4 weeks. Fluorescence micrographs of the mineralized PCG NF fragments after (C) E7-BMP-2-FITC peptide loading and (D) 28 days of release.

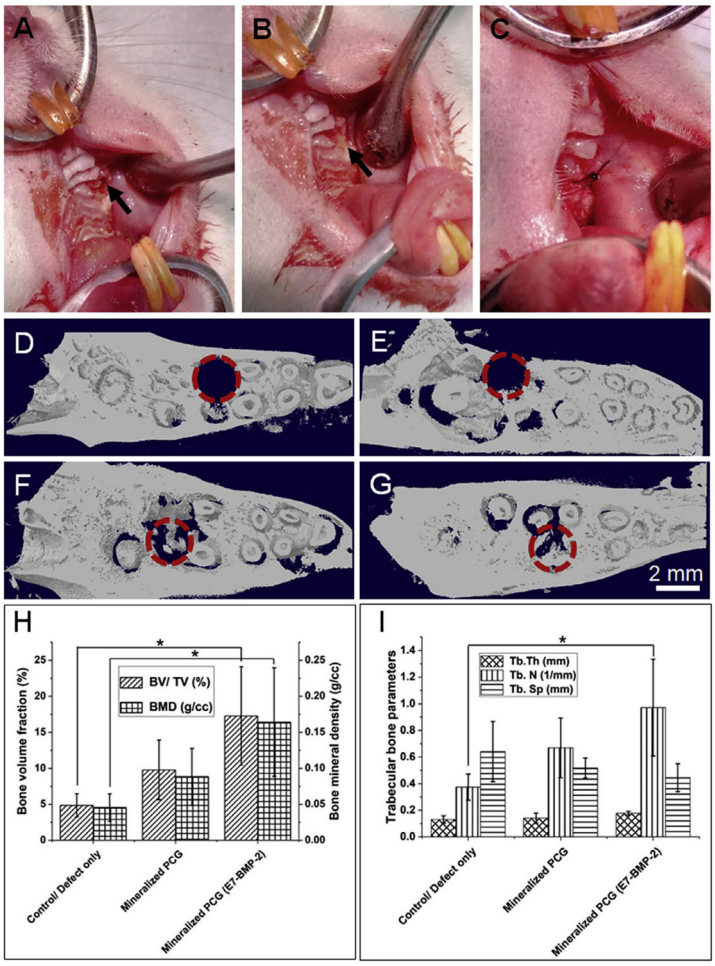

Fig. 4.

Intraoperative image of the critical-sized defect created in rat maxillae (upper jaw) after extraction of the first molar tooth. (A) Defect drilled into the upper jaw bone (indicated by arrow), (B) Filling of defect with mineralized nanofiber graft, and (C) Suturing of the tissue around the defect to hold the graft in place. Representative 3D reconstructions of coronal (XZ) view micro-CT images of the defect (D) immediately after tooth extraction and defect creation, (E) Unfilled defect/control after 4 weeks, (F) Defect filled with mineralized PCG nanofiber fragments, and (G) Defects filled with E7-BMP-2 peptide-loaded mineralized PCG nanofiber fragments. The dashed circles indicate the region of the defect. (H) New bone volume fraction (%) and bone mineral density (g/cc), and (I) trabecular bone parameters (thickness, number, and separation) measured in the different experimental groups after 4 weeks of suturing the periodontal defects. Data shown are mean ± SD of n = 6 for each group. *$p < 0.05$.

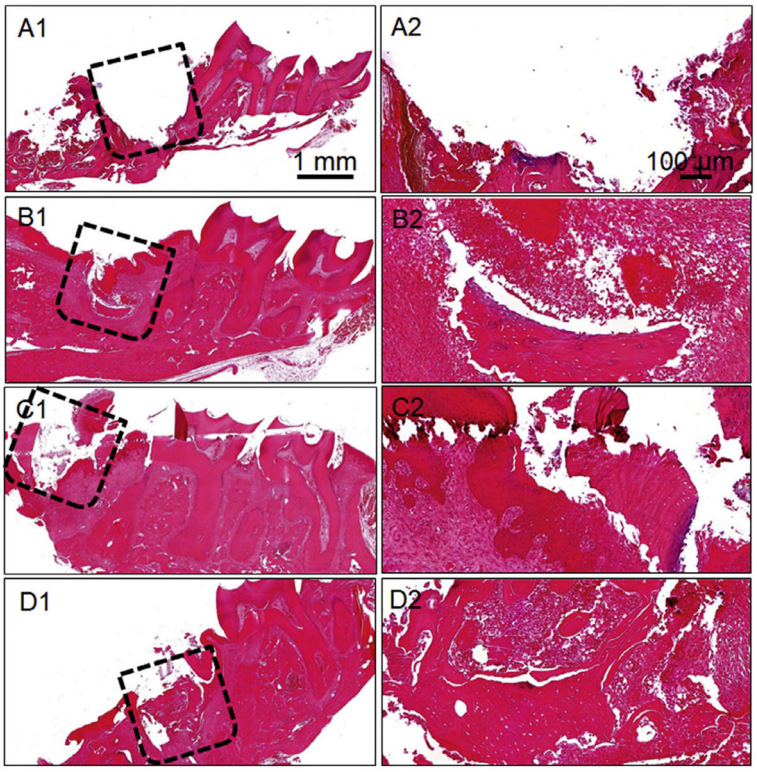

Fig. 5.

Hematoxylin and eosin-stained images of different experimental groups studied for periodontal bone healing. (A1/A2) Immediately after tooth extraction and defect creation, (B1/B2) Unfilled defect/control after 4 weeks of surgery, (C1/C2) Mineralized PCG nanofiber fragments after 4 weeks of graft implantation, and (D1/D2) E7-BMP-2- loaded mineralized PCG nanofiber fragments after 4 weeks of graft implantation. The dashed boxes indicate the defect region.

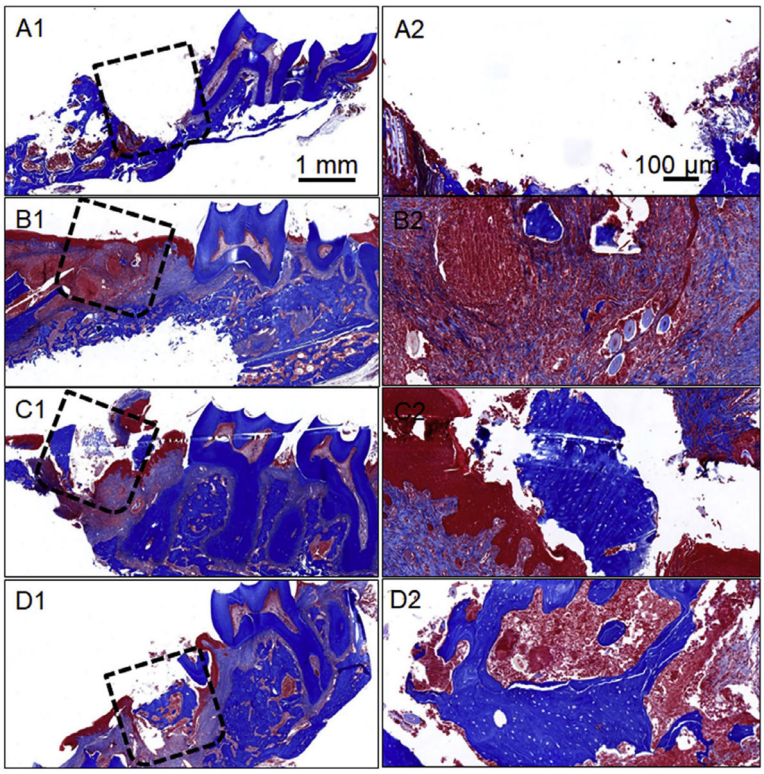

Fig. 6.

Masson's trichrome-stained images of different experimental groups studied for periodontal bone healing. (A1/A2) Immediately after tooth extraction and defect creation, (B1/B2) Unfilled defect/control after 4 weeks of surgery, (C1/C2) Mineralized PCG nanofiber fragments after 4 weeks of graft implantation, and (D1/D2) E7-BMP-2- loaded mineralized PCG nanofiber fragments after 4 weeks of graft implantation. The dashed boxes indicate the defect region.